

Short Communication

Temperature Control in the Formation of Bimetallic Metal-doped Nanoporous Carbon as a Sulfur Host for Long-Life Lithium–Sulfur Batteries

Yifan Zheng¹, Wangjun Feng^{1*}, Linjing Chen¹

¹School of Science, Lanzhou University of Technology, Lanzhou 730050, China

*E-mail: wjfeng@lut.cn

Received: 30 April 2020 / Accepted: 27 June 2020 / Published: 10 August 2020

BMZIFs were synthesized by room-temperature reaction of a $\text{Zn}(\text{NO}_3)_2$ and $\text{Co}(\text{NO}_3)_2$ mixture solution and 2-methylimidazole. Furthermore, thermal treatment enabled improvement of the electrochemical properties of the materials. To investigate the optimum carbonization temperature for the BMZIFs, we conducted a thermal treatment experiment to explore the role of different temperatures. The sample morphology was characterized by scanning electron microscopy. Electrochemical characterization was examined by cyclic voltammetry and galvanostatic charge–discharge tests. Based on these electrochemical experiments, a sample treated at 900°C was found to show excellent electrical conductivity; the initial discharge capacity of a lithium–sulfur battery using Co,Zn-C-900@S as the electrode material was determined to be 1100.2 mAh/g at 0.1C. This shows that Co,Zn-C-900@S exhibits the best electrochemical performance characteristics.

Keywords: Lithium-sulfur battery; Metal–organic framework, Bimetallic ZIFs; MOF-derived porous carbon; Thermal Treatment

1. INTRODUCTION

Lithium-sulfide batteries have shown high commercial potential in recent years[1-3], but there are some technical problems that limit their development. First, the low conductivity of sulfur and final discharge products leads to a low specific capacity for lithium sulfide batteries. Second, a “shuttle reaction” between the positive electrode and negative electrode reduces the sulfur positive material and destroys the negative electrode structure. Finally, a collapse of the sulfur positive matrix in the process of charging and discharging reduces the battery life[4-7]. To solve these problems, researchers have prepared a type of carbon-based composite materials, which have high specific surface area and good electronic conductivity, which can be composited with sulfide as the positive electrode[8-11]. However, these designs are limited by weak interactions between the carbon scaffolds and sulfur, which are based

only on physical adsorption[12]. To date, it has been demonstrated that heteroatom doping (e.g., N, B, P, Co, Fe, etc.)[13-17] within the porous carbons forms NPC, which is powerful in improving the electronic properties and conductivity. When the interaction between the heteroatom ions and sulfur ions is used for chemical adsorption and combined with the physical adsorption of carbon materials, the structural stability of the cathode can be greatly enhanced, to improve the specific capacity and cycle performance of the battery[14-19].

MOF-derived porous carbon materials are a valid form of NPC[20-24]. MOF was first discovered by Liu et al. and is a kind of microporous material that is self-assembled by metal ions and organic coordination, with heteroatoms loaded into the organic structure to ensure that the heteroatoms exist uniformly and stably. Thus, the morphology of this material is highly controllable and shows a denser structure. By further pyrolysis of MOF precursors, the long-term ordering and high porosity of MOFs can be partly retained to obtain well-organized skeleton porous carbon with high specific surface area[25]. Zeolitic imidazolate frameworks (ZIFs) are a kind of MOFs[26]. Among the ZIF series, Zn-ZIF-8 and Co-ZIF-67 are two kinds of microporous structures commonly used as carbide materials. Chen et al. reported a bimetallic ZIF (BMZIF) material based on Zn-ZIF-8 and Co-ZIF-67, which was obtained through the use of different Co/Zn ratios. According to this study, BMZIFs show a very high specific surface area, high graphitization of carbon and a wide and even distribution of N, Co-N_x keys. Their research also studied the influence of the Co/Zn ratio in BMZIF and found that when the Co/Zn ratio reached 20:1, the material showed the best performance. This improvement not only expands the specific surface area and enhances the electric conductivity and physical absorbability of the host material but also combines the critical Co(Fe)-N_x sites with polysulfide ions, resulting in very strong chemical absorbability. Therefore, the battery charging and discharging capacity and capacity retention rate can be greatly improved at the same time. As we know, the electrical performance of each metal-organic framework is closely related to the temperature of carbonization. However, in their research, Chen et al. did not especially discuss the effect of temperature on materials, but just set the carbonization temperature of BMZIF at certain 900°C, which may not be the most suitable temperature.

In this regard, we investigate the relation between the carbonization temperature and electrical performance, and attempt to ascertain the optimal temperature at which the carbonization produces the best effective BMZIF. We set five temperature points between 600°C and 1000°C, from which the best temperature is determined.

2. EXPERIMENTAL DETAILS

2.1 Materials

Cobalt nitrate hexahydrate (98%, Aladdin), zinc nitrate hexahydrate (98%, Aladdin) and 2-methylimidazole (99%, Aladdin) were used without further treatment.

2.2. Preparation of the BMZIF

The synthesis of BMZIF has been discussed in previous research[10]. Typically, Zn (NO₃)₂·6H₂O (1.566 g) and Co(NO₃)₂·6H₂O(0.800 g) were mixed with Zn²⁺/Co²⁺ at a mole ratio of 20:1 and dissolved into 80 ml methanol to form a homogeneous solution A; then, 3.7 g 2-methylimidazole was added to 80 ml methanol to form solution B, which was subsequently mixed with solution A followed by vigorous stirring at room temperature for 24 h. After being washed alternately with deionized water and methanol several times, a lilac deposit was obtained by centrifugal collection, which was finally dried overnight in vacuum at 50°C. The BMZIF powder was reactivated at 200°C for 24 hours before use.

2.3 Preparation of the Co,Zn-C-n

The activated BMZIF powder was respectively heated to 600°C, 700°C, 800°C, 900°C, 1000°C at a heating rate of 5°C/min for 2 hours. The activated BMZIF powder was carbonized in a N₂ environment and naturally cooled to room temperature to obtain the porous carbon material. Samples were labelled as Co,Zn-C-n, where n represents the carbonization temperature, i.e., Co,Zn-C-600, Co,Zn-C-700, Co,Zn-C-800, Co,Zn-C-900 and Co,Zn-C-1000.

2.4 Preparation of the Co,Zn-C-n@S Composites

The obtained Co,Zn-C-n samples were mixed with sulfur powder at a weight ratio of 4:6 and then evenly ground. Then, the samples were heated in an argon atmosphere at 155°C for 20 h to obtain the Co,Zn-C-n@S materials. The sample, Super P and aqueous binder (LA133) were then all mixed together at a weight ratio of 7:2:1. Next, the viscous liquid was spread onto conductive aluminium foil and then dried overnight in vacuum at 55°C. To evaluate the electrochemical performance of the new Co,Zn-C-n@S structure, 2025-type coin cells were assembled using lithium metal foil as the counter electrode. The static charge and discharge period was measured using a land CT 2001A battery test system with a cut-off voltage window of 1.7 V-2.8 V.

2.5 Materials characterization

X-ray diffraction (XRD) patterns were recorded by a Bruker D8 Advance diffractometer using Cu K α radiation from 10° to 80°. The morphological characterization of the composite materials was studied by scanning electron microscopy (SEM; JSM-6700F, JEOL, Tokyo, Japan) at 20 kV.

3. RESULTS AND DISCUSSION

The synthesis process for BMZIF is shown in Figure 1. Zn (NO₃)₂·6H₂O and Co(NO₃)₂·6H₂O were first mixed at a Zn/Co mole ratio of 20:1. Then, a Co,Zn-doped polyhedron was generated by pyrolysis reaction. Finally, different Co,Zn-C-n@S materials were obtained by carbonization at different temperatures.

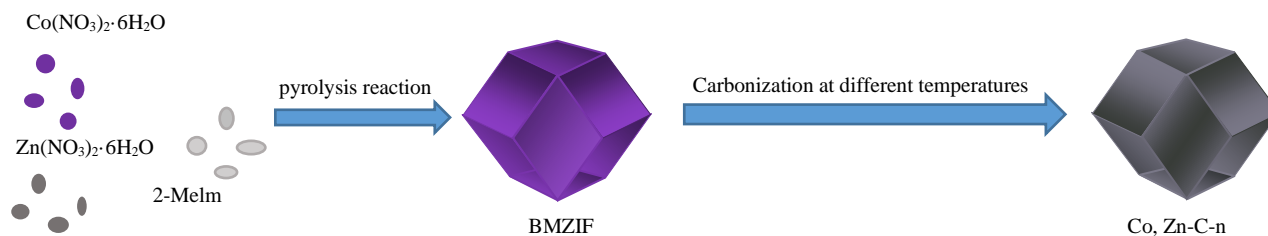


Figure 1. Schematic diagram of the synthesis process for Co,Zn-C-n

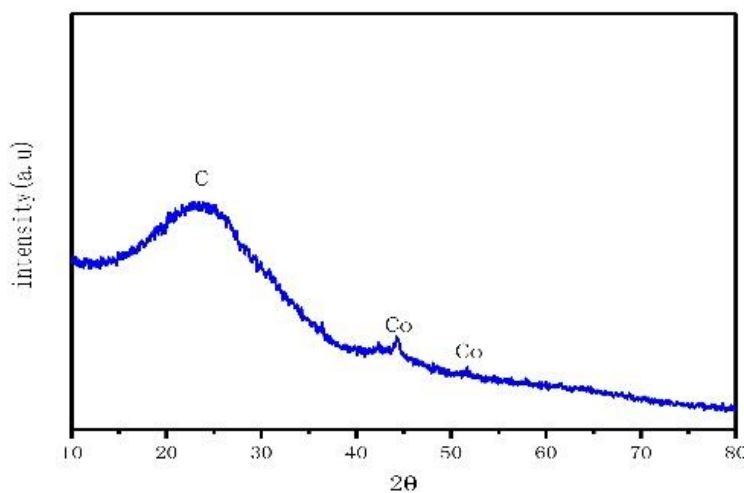


Figure 2. XRD patterns for the Co,Zn-C-900 material

Figure 2 shows the XRD patterns obtained for the Co,Zn-C-900 material, which shows the crystallographic phases present in the Co,Zn-C-900 material. This result is consistent with the reported simulation model; that is to say, Co,Zn-C-900 was successfully realized. Four peaks can be seen clearly in this map; among these peaks, two sharp peaks are found at 25° and 44°, which were respectively indexed to the (002) and (101) diffractions of carbon. The other two peaks at 44° and 51° can be respectively assigned to the (111) and (200) diffraction of fcc Co, which is formed from Co nanoparticles inset into the carbon shell. These results are identical to those obtained by Chen et al., which proves the successful synthesis of Co,Zn-C-900. We compared the results obtained for Zn-ZIF-8[27] and Co-ZIF-67[14], which are formed under the optimal carbonization temperature and correspond to Zn-C-800 and Co-C-900, respectively, and found that Co,Zn-C-900 shows higher carbon peaks than the Co-C-900 materials. This fully indicates that Co,Zn-C-900 has a higher carbonization degree than Co-C-900, which can fully carry sulfur and improve the conductivity of the electrodes. Then, the results were compared with Zn-C-800. Co-Zn-900 shows an extra cobalt peak, which indicates that cobalt nanoparticles are added to the Co, Zn-C-900, which enhance the chemisorption capacity of the polysulfide ions and electrode materials in the charging and discharging process, thus improving the cycling performance of the electrode.

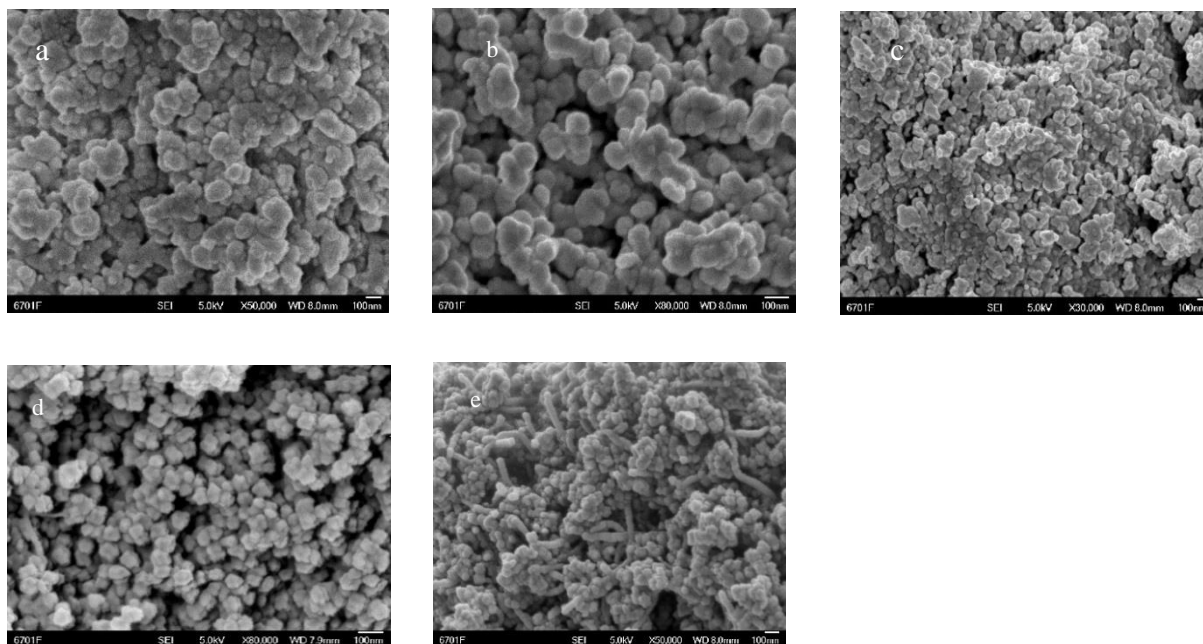


Figure 3. SEM images of (a) Co, Zn-C-600 (b) Co, Zn-C-700 (c) Co, Zn-C-800 (d) Co, Zn-C-900 and (e) Co, Zn-C-1000

Figure 3 shows the SEM images of different Co, Zn-C-n materials, which shows the microstructure morphology of Co, Zn-C-n. The materials formed using different carbonization temperature ranging from 600°C to 900°C retain the same homogeneous polyhedral shape. The skeletal structures show a little shrinkage because of the thermal effect, which can be seen in Figure 3a-3d. When the carbonization temperature is increased, the skeletal structure becomes shrivelled accordingly. This phenomenon of increased shrinkage for the metal organic skeleton with increasing temperature not only exists in this experiment but also exists for Zn-ZIF-8 and Co-ZIF-67. The structure proves that the material generated at the carbonization temperature of 900° has the best morphology, showing obvious polyhedron particles, a complete structure, and a particle size of 30 nm, which is smaller than the size of Zn-ZIF-8 and Co-ZIF-67. As shown in Figure 3e, when the carbonization temperature reaches 1000°C, the morphology of the material is destroyed to a certain degree and is even changed to an elongated tubular structure in the worst-case scenario.

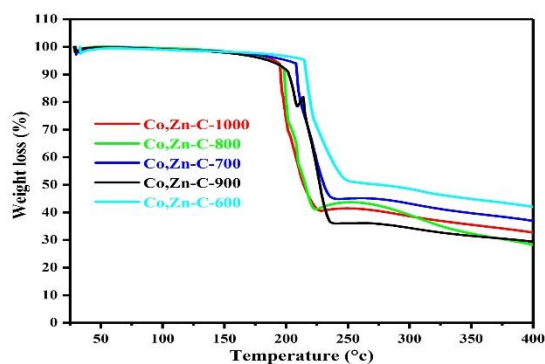


Figure 4. Thermogravimetric analysis (TGA) of the different Co, Zn-C-n materials

Figure 4 shows the thermogravimetric analysis (TGA) for the different Co, Zn-C-n materials, which was performed in the temperature range of $15^{\circ} \sim 400^{\circ}\text{C}$ at a heating rate of $5^{\circ} \text{C min}^{-1}$ in N_2 to determine the weight content of sulfur. As shown in Figure 4, Co,Zn-C-900@S has a high loading ratio, which is significantly higher than that in the other Co, Zn-C-n@S. In addition, the higher sulfur evaporation temperature ($200^{\circ}\text{-}400^{\circ}\text{C}$) indicates stronger absorption of sulfur.

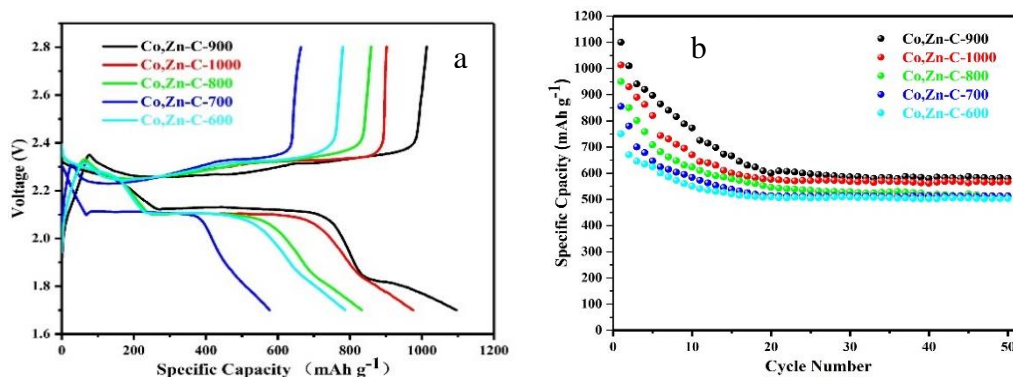


Figure 5. (a) Initial charge–discharge profiles for the ZIF-sulfur cathode at 0.1C; (b) cycling performance of the Co, Zn-C-n@S composites at 0.2C

Figure 5(a) shows the initial charge–discharge profiles for the different Co, Zn-C-n materials. The first discharge platform (2.3 V–2.1 V) corresponds to the reaction from high-order lithium polysulfide (Li_2S_8) to low-order lithium polysulfides (Li_2S_x , $4 \leq x \leq 8$). The second discharge platform corresponds to the process from low-order lithium polysulfides (Li_2S_x , $4 \leq x \leq 8$) to lithium disulfide or lithium sulfide (Li_2S_2 or Li_2S), alternatively. It can be seen that at 0.1C, the initial discharge capacities for Co, Zn-C-600 to Co, Zn-C-1000 were 598.3 mAh g^{-1} , 797.6 mAh g^{-1} , 830.5 mAh g^{-1} , 996.5 mAh g^{-1} and $1100.2 \text{ mAh g}^{-1}$, respectively. The use of the Co,Zn-C-900 material processed at a carbonization temperature of 900°C leads to the highest initial battery capacity, which corresponds to the material with the most perfect structure in the SEM images. This is consistent with the optimal carbonization temperature for Co-ZIF-67, but higher than that for Zn-ZIF-8. Figure 5(b) shows the long-term cycle performance of different Co, Zn-C-n@S materials at a current density of 0.2C. By comparing several materials, one finds that Co,Zn-C-900 shows the best electrochemical properties, with the specific capacity reaching 1098 mAh/g . This capacity is obviously better than that obtained for Zn-C-800 Co-Zn-900, which further demonstrates the advantages of using BMZIF as the electrode host; the electrochemical performance of Co,Zn-C-600, Co,Zn-C-700, Co,Zn-C-800, Co,Zn-C-1000 in terms of specific capacity is 753.2 mAh g^{-1} , 854.4 mAh g^{-1} , 952.3 mAh g^{-1} , $1024.3 \text{ mAh g}^{-1}$, respectively. The initial capacity increases with increasing temperature, which is also reflected in the other ZIFs. This indicates that the performance of the material is determined by the structural integrity, which is clearly affected by the temperature of carbonization. The performance of the battery is the best for the case of high carbonization and perfect material structure.

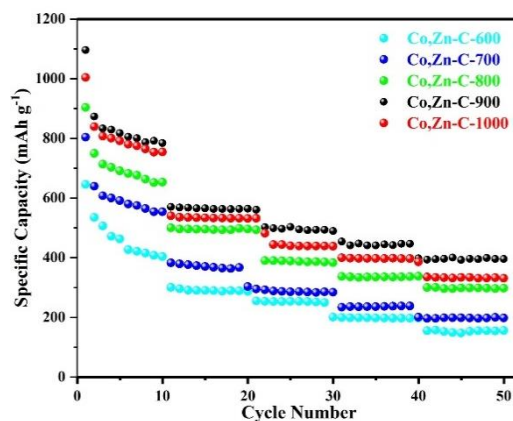


Figure 6. Rate capability of Co-Zn-C-n@sulfur composites at various current densities ranging from 0.1C to 3C

Figure 6 shows the effect of increasing discharge rate from 0.1 C to 3C on the specific capacity for Co, Zn-C-n@S, which was conducted at various current densities (0.1C, 0.2C, 0.5C, 1.0C, 2.0C and 3.0C) after 10 cycles. It can be seen that with increasing carbonization temperature, the multiplier performance is significantly improved; however, after the carbonization temperature exceeds 900 °C, the material structure is destroyed and the performance declines. Generally, the material performance is the best obtained at a carbonization temperature of 900 °C. As seen from Figure 6, when the current is at 0.1C, the initial capacity of Co,Zn-C-900@S reaches 1098.7 mAh/g, which is significantly higher than that found for the other materials. In addition, compared with the best carbonized materials for Zn-C-800, Co-Zn-900, Co,Zn-C-900 shows the highest initial capacity. When the current is increased to 3C, the capacity of Co,Zn-C-900@S can still be maintained at 500.3 mAh/g, which is also higher than that found for the other materials. This capacity is also higher than that obtained for the best carbonized material for Zn-C-800, Co-Zn-900, which further indicates that Co,Zn-C-900 has good cycling performance. XRD, SEM and Cycling performance at 0.1c after 50 Cycles are compared in Table 1 to further illustrate the superior performance of Co-Zn-C-900 material.

Table 1. Comparison with other currently reported carbon materials

Material	XRD	Size in SEM	Cycling performance at 0.1C after 50 cycles	Reference
Zn-C-800	Shows higher carbon peaks,don't have cobalt peak	300nm	300 mAhg ⁻¹	27
Co-C-900	Shows cobalt peak,don't have higher carbon peaks	50nm	400 mAhg ⁻¹	14
Zn-Co-C-900	Both have cobalt peak and higher carbon peaks	30nm	Not Given	10
Zn-Co-C-900	Both have cobalt peak and higher carbon peaks	30nm	500 mAhg ⁻¹	This work

4. CONCLUSION

A bimetallic metal organic framework based on a hollow polyhedron was successfully prepared by solvothermal reaction and then further treated by carbonization at different temperatures to form carbon materials with various characteristics. Through analysis by SEM, Co-Zn-C-900 was found to show a complete carbonized frame. These results were confirmed through several electrochemical characterization experiments. As an ideal battery candidate, Co,Zn-C-900 was found to show good rate and cycle stability. The capacity retention for this material also exhibited an enhanced value compared to the other samples. To summarize the results obtained in this study, effective thermal treatment for BMZIFs used as lithium-sulfur electrodes can improve not only the specific capacity and electroconductivity but also sulfur reaction utilization and cycling stability.

FUNDING INFORMATION

This work was financially supported by the National Natural Science Foundation of China (Grant No. 21965019)

References

1. G. Gao, W. Feng, W. Su, S. Wang, L. Chen, M. Li, C. Song, *Int. J. Electrochem. Sci.*, 15(2020)1426-1436.
2. M. Li, W. Feng, W. Su, X. Wang, *Int. J. Electrochem. Sci.*, 15(2020)526.
3. C. Song, W. Feng, X. Wang, Z. Shi, *Ionics*, 26 (2020)661.
4. C. Song, W. Feng, X. Wang, Z. Shi, *Journal of Electroanalytical Chemistry*, 862 (2020) 113962.
5. L. Yin, J. Wang, F. Lin, J. Yang, Y. Nuli, *Energy Environ. Sci.*, 5 (2012) 6966.
6. R. Elazari, G. Salitra, Y. Talyosef, J. Grinblat, C. Scordiliskelley, A. Xiao, & D. Aurbach, *Energy Environ. Sci.*, 3 (2010)1131.
7. J.-G. Wang, K. Xie, B. Wei, *Nano Energy*, 15 (2015) 413-444.
8. Y. Zhao, W. Wu, J. Li, Z. Xu, L. Guan, *Adv. Mater.*, 26 (2014) 5113-5118.
9. M. Hagen, S. Dorfler, H. Althues, J. Tubke, M.J. Hoffmann, S. Kaskel, & K. Pinkwart. *Journal of Power Sources*, 213(2012)239.
10. H. Zhou, S. Zhu, M. Hibino, I. Honma, M. Ichihara, *Adv. Mater.*, 15 (2003) 2107-2111.
11. X. Ji, K.T. Lee, L.F. Nazar, *Nat. Mater.*, 8 (2009) 500-506.
12. Y.-Z. Chen, C. Wang, Z.-Y. Wu, Y. Xiong, Q. Xu, S.-H. Yu, H.-L. Jiang, *Adv. Mater.*, 27 (2015) 5010-5016.
13. W. Zhou, C. Wang, Q. Zhang, H.D. Abruña, Y. He, J. Wang, S.X. Mao, X. Xiao, *Adv. Energy Mater.*, 5 (2015) 1401752.
14. Z. Li, C. Li, X. Ge, J. Ma, Z. Zhang, Q. Li, C. Wang, L. Yin, *Nano Energy*, 23 (2016) 15-26.
15. X. Li, L. Pan, Y. Wang, C. Xu, *Electrochimica Acta*, 190 (2016) 548-555.
16. X. Zou, R. Silva, A. Goswami, T. Asefa, *Appl. Surf. Sci.*, 357 (2015) 221-228.
17. B. Wang, Y. Zhu, W. Ren, J. Wang, H. Guo, *Phys. Rev. B*, 75 (2007) 235415.
18. F. Pei, T. An, J. Zang, X. Zhao, X. Fang, M. Zheng, Q. Dong, N. Zheng, *Adv. Energy Mater.*, 6 (2016) 1502539.
19. N.L. Torad, M. Hu, S. Ishihara, H. Sukegawa, A.A. Belik, M. Imura, K. Ariga, Y. Sakka, Y. Yamauchi, *Small*, 10 (2014) 2096-2107.
20. L. Zhang, Z. Su, F. Jiang, L. Yang, J. Qian, Y. Zhou, W. Li, M. Hong, *Nanoscale*, 6 (2014) 6590-6602.
21. K. Xi, S. Cao, X. Peng, C. Ducati, R. Vasant Kumar, A.K. Cheetham, *Chem. Commun.*, 49 (2013)

- 2192.
22. S. Bai, K. Zhu, S. Wu, Y. Wang, J. Yi, M. Ishida, H. Zhou, *J. Mater. Chem. A*, 4 (2016) 16812-16817.
 23. X. Feng, X. Bo, L. Guo, *J. Power Sources*, 389 (2018) 249-259.
 24. G. Xu, B. Ding, L. Shen, P. Nie, J. Han, X. Zhang, *J. Mater. Chem. A*, 1 (2013) 4490.
 25. L. Fan, H. Wu, X. Wu, M. Wang, J. Cheng, N. Zhang, Y. Feng, K. Sun, *Electrochimica Acta*, 295 (2019) 444-451.
 26. K. Li, D.H. Olson, J. Seidel, T.J. Emge, H. Gong, H. Zeng, J. Li, *J. Am. Chem. Soc.*, 131 (2009) 10368-10369.
 27. M. Li, Y. Wan, J.-K. Huang, A.H. Assen, C.-E. Hsiung, H. Jiang, Y. Han, M. Eddaoudi, Z. Lai, J. Ming, L.-J. Li, *ACS Energy Lett.*, 2 (2017) 2362-2367.
 28. J.-Y. Hong, Y. Jung, K.-M. Kim, S. Kim, *J. Nanosci. Nanotechnol.*, 18 (2018) 279-283.

© 2020 The Authors. Published by ESG (www.electrochemsci.org). This article is an open access article distributed under the terms and conditions of the Creative Commons Attribution license (<http://creativecommons.org/licenses/by/4.0/>).